Structural and optical properties of copper-coated substrates for solar thermal absorbers

Superlattices and Microstructures 98 (2016) 342–350

Contents lists available at ScienceDirect

Superlattices and Microstructures

journal homepage: www.elsevier.com/locate/superlattices

Structural and optical properties of copper-coated substrates for solar thermal absorbers

Stefano Pratesi [a], Maurizio De Lucia [a], Marco Meucci [b], Elisa Sani [b, *]

[a] DIEF Dipartimento di Ingegneria Industriale, Università degli Studi di Firenze, Via di S.Marta, 3, I-50139 Firenze, Italy
[b] CNR-INO National Institute of Optics, Largo E. Fermi, 6, I-50125 Firenze, Italy

ARTICLE INFO

Article history:
Received 17 August 2016
Accepted 19 August 2016
Available online 26 August 2016

Keywords:
Black chrome
Copper coating
Optical properties
Concentrating solar power
Linear parabolic collectors
Parabolic trough collectors

ABSTRACT

Spectral selectivity, i.e. merging a high absorbance at sunlight wavelengths to a low emittance at the wavelengths of thermal spectrum, is a key characteristics for materials to be used for solar thermal receivers. It is known that spectrally selective absorbers can raise the receiver efficiency for all solar thermal technologies. Tubular sunlight receivers for parabolic trough collector (PTC) systems can be improved by the use of spectrally selective coatings. Their absorbance is increased by deposing black films, while the thermal emittance is minimized by the use of properly-prepared substrates. In this work we describe the intermediate step in the fabrication of black-chrome coated solar absorbers, namely the fabrication and characterization of copper coatings on previously nickel-plated stainless steel substrates. We investigate the copper surface features and optical properties, correlating them to the coating thickness and to the deposition process, in the perspective to assess optimal conditions for solar absorber applications.

1. Introduction

The use of a low-intensity source like sunlight for energy generation requires an efficient system to concentrate and capture radiation and to transfer the energy to the exchange fluid. Sunlight is abundant, renewable and free of charge. Therefore the development and diffusion of solar energy exploitation is a key issue for the future. However, at present solar energy technologies are generally affected by an efficiency not high enough and by a high cost, making them not fully competitive over conventional fossil fuels yet. Thus, it is clear that both increasing the efficiency and reducing the cost is mandatory to promote solar energy exploitation. Materials utilized in different solar collector architectures are selected according to the required working temperature [1] and especially the material constituting the receiver is a key component for all collector schemes [2]. Systems operating at mid-temperatures (i.e. using fluids at about 200 ÷ 300 °C) and in particular parabolic trough collectors (PTCs) offer several advantages in comparison with conventional flat plates thanks to their higher efficiency and reduced receiver surface. In these systems the incident solar radiation is converted into heat either by direct absorption in a heat transfer fluid flowing trough transparent tubes (a black liquid [3] and, more recently, a nanofluid [4–9]) or, in the majority of cases, by sunlight absorption by blackened or specially developed absorbing surfaces that collect the solar energy and transfer it to the fluid. The characteristics which are required to the absorber surface are chemical and physical stability at the operating temperatures and good performances in terms of energy efficiency.

* Corresponding author.
E-mail address: elisa.sani@ino.it (E. Sani).

http://dx.doi.org/10.1016/j.spmi.2016.08.031
0749-6036/

Moreover a production process characterized by a low cost and a high repeatability is highly desired, as it should promote a large scale diffusion. Several direct industrial applications, like Direct Steam Generation (DSC) and Solar Heating and Cooling (SHC), could exploit mid-temperature solar energy as energy source. This interest drives the research of novel technologies focused on this market sector where the technologies developed for systems operating at higher temperatures (e.g. CSP plants) cannot be used.

Electrodeposition techniques are a promising route to obtain surfaces with tailored optical characteristics and are known in particular for coloring metallic substrates [10]. Black nickel coatings have excellent optical properties, as they are strongly absorbing in the sunlight spectral region, with a high absorbance $\alpha \approx 0.88 \div 0.96$ and a low thermal emittance $\varepsilon \approx 0.10 \div 0.15$, but they are not physically and chemically stable at temperatures T > 200 °C [11,12]. Black chrome coatings show a slightly lower sunlight absorption in comparison with black nickel ($\alpha \approx 0.90 \div 0.92$; $\varepsilon \approx 0.10 \div 0.15$) but they remain stable up to 300 °C [13]. However, a relevant drawback correlated to chrome electrodeposition is represented by pollution derived from Cr^{6+} ions [14,15]. Because of that, the technological development of these processes underwent a sharp slowdown since '90 [16–18]. Only with the advent of new studies about Cr^{3+} baths, since the beginning of 2000's, the electrodeposition processes have found new interest in mass production of components for thermal solar plants. To obtain a good coating by black chrome, a preliminary deposition of a nickel layer on the substrate is needed to ensure a better chrome adherence to the surface [19] and an improved wear and corrosion resistance [20]. Moreover this creates an "absorber/reflector tandem" having both the high solar absorbance of the black exterior deposit and the low thermal emittance of the metallic inner coating [20]. Recently we investigated morphological and optical properties of nickel substrates [21]. However, copper coatings are known to be possible substrates for black chrome depositions as well [17,22,23]. In addition, preliminary tests have shown that obtaining black chrome deposition on copper is very easy and that the black layer has great uniformity and adherence. For this reason, in the present work we show the realization and systematic study of copper substrates, aimed to assess their suitability as low-emittance intermediate coating for further black chrome deposition. We investigated morphological and optical properties as a function of the bath parameters and coating thickness.

2. Experimental

Substrates for copper electrodeposition have been chosen to be stainless steel AISI 304 samples with a preliminary nickel coating (Wood bath for Ni [21], 0.9 μm Ni thickness). The composition of Cu sulphate acid bath [25,26] was $CuSO_4 \cdot 5H_2O$ 225 g l^{-1} and H_2SO_4 concentrated 33 g l^{-1}. Other parameter were: laminated Cu anodes, room temperature, current density 2–5 A dm^{-2}. In detail, two consecutive depositions have been carried out, the first one for times from 0.5 to 14 min with current density 3.45 A dm^{-2} (results shown in Fig. 1), and the second one with 0.51 A dm^{-2} for 5 and 10 min, as proposed in Ref. [27].

Thicknesses have been measured with Calotest CSM and optical microscope Nikon Eclipse LV 150, by means of the image analysis. Structural characterization has been performed using a scanning electron microscope SEM "Zeiss Merlin". A Hommel Tester W55 (Jenoptic) has been used for measuring the roughness. The hemispherical reflectance spectra from 0.25 to 16 μm wavelength have been acquired using two experimental apparatuses: a double-beam spectrophotometer (Lambda 900 by Perkin Elmer) equipped with a 150 mm diameter Spectralon®-coated integration sphere for the 0.25–2.5 μm wavelength region (this setup is also suitable for measuring the purely diffuse reflectance and thus obtaining the specular component as a difference) and a FT-IR "Excalibur" Bio-Rad spectrophotometer, equipped with a gold-coated integrating sphere and a liquid nitrogen cooled detector for the wavelength region 1.8–16 μm. For diagnostic purposes we acquired also the specular reflectance spectra of samples, extending the investigated spectral region up to 40 μm wavelength. The Excalibur spectrometer, equipped with the proper accessory for specular reflectance measurements, allows to reach 25 μm

Fig. 1. Cu-coated samples for current density 3.45 A dm^{-2}, deposition time 1 min.

wavelength. For longer wavelengths we used a FT-IR "Scimitar" Bio-Rad spectrometer with the same specular reflectance accessory.

3. Results and discussion

3.1. Thickness characterization

As reported in Ref. [27], the electrodeposition efficiency for Cu is 100%. Therefore it is possible to calculate the expected coating thickness by the knowledge of deposition time and current density. The involved chemical reaction is:

$$Cu^{2+} + 2e^{-} \rightarrow Cu^{0}$$

thus $2e^{-}$ are required for reducing each Cu^{2+} ion to metallic Cu.

For a current density of 3.45 A dm^{-2}, the expected thickness grow rate is 0.45 μm min^{-1}, while for density 0.51 A dm^{-2} we expect a thickness of 0.07 μm min^{-1}.

The samples have all undergone the same preliminary Wood-type Ni deposition. As for the copper coating, deposition times are 0.5–14 min (3.45 A dm^{-2} current density) and 5–10 min for 0.51 A dm^{-2}. To evaluate possible non-homogeneous current distribution effects, if any, for each sample we measured the Cu thickness on both front and back faces, (labeled as *f* and *b*, respectively). The results are listed in Table 1. In addition, for a more significant assessment of the relationship between deposition parameters and coating thickness, for each group of samples obtained with the same deposition parameters (deposition time and current density), we calculated the average thickness value: this result is shown in Figs. 2–3 and confirms the expected linear dependence of the Cu thickness on both deposition time and transferred charge. If we observe the thickness values in Table 1 for similar deposition times, some spread of values can be appreciated. This can be more reasonably ascribed to the intrinsic difficulty of the Calotest measurement rather than a poor repeatability of the bath, as, in any case, it is possible to see from Fig. 2 that the theoretically expected time dependence of thickness is confirmed. Therefore, if we consider that, as already said, the efficiency of Cu deposition is 100%, we can define as uncertainty on the Calotest

Table 1
Results of Calotest thickness measurement. *f* and *b* label the front and the back face of each sample. For some specimens the number of significant digits in thickness measurement is lower due to the difficulty to measure the dimensions of craters.

Sample	t_{dep} min	Thickness μm	Sample	t_{dep} min	Thickness μm
70f	0.5	0.4	446f	3	1.69
71b	0.5	0.3	446b	3	1.55
58fc1	1	0.6	447f	3	1.35
58fc2	1	0.6	447b	3	1.32
58fc3	1	0.6	448f	3	1.68
58b	1	0.5	448b	3	1.10
59f	1	0.5	449f	3	1.80
59b	1	0.6	449b	3	1.13
438f	1.5	0.87	450f	7	4.14
438b	1.5	0.84	450b	7	3.61
439f	1.5	0.66	451f	7	3.12
439b	1.5	0.65	451b	7	2.96
440f	1.5	0.71	452f	7	4.01
440b	1.5	0.59	452b	7	2.42
441f	1.5	0.77	453f	7	4.15
441b	1.5	0.65	453b	7	2.70
62f	2	2.0	454f	14	8.56
62b	2	0.9	454b	14	7.38
63f	2	1.4	455f	14	6.92
63b	2	1.4	455b	14	6.41
64f	2	1.4	456f	14	7.66
64b	2	1.2	456b	14	5.94
65f	2	1.4	457f	14	8.11
65b	2	1.3	457b	14	6.23
442f	2.5	1.49	74f	5	0.5
442b	2.5	1.31	74b	5	0.4
443f	2.5	1.03	460f	10	1.88
443b	2.5	1.13	460b	10	1.47
444f	2.5	1.33	461f	10	0.7
444b	2.5	0.88	461b	10	1.52
445f	2.5	1.53			
445b	2.5	1.03			

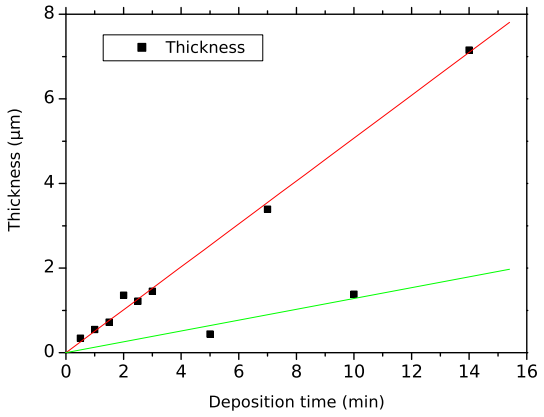

Fig. 2. Thickness of the Cu coating (average on the deposition time) as a function of the deposition time. Red line represents the linear fit of data relative to the samples made with J = 3.45 A dm^{-2}, whereas the green line represent the linear fit of the data relative to the samples made with J = 0.51 A dm^{-2}. (For interpretation of the references to colour in this figure legend, the reader is referred to the web version of this article.)

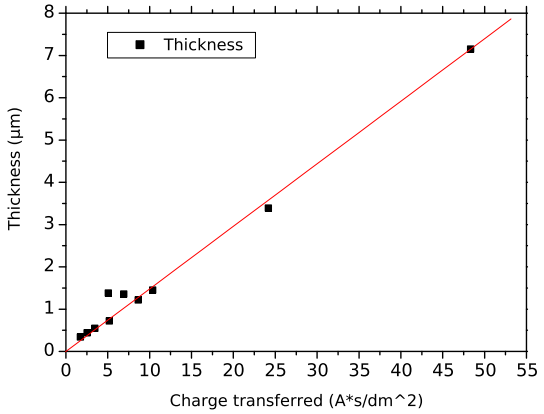

Fig. 3. Thickness of the Cu coating (average on the transferred charge) as a function of the transferred charge. Red line represents the linear fit of data: as we can see the deposition efficiency of the processes at J = 3.45 A dm^{-2} and J = 0.51 A dm^{-2} is the same. (For interpretation of the references to colour in this figure legend, the reader is referred to the web version of this article.)

thickness measurement the difference between theoretical and experimental growth rates, which in our case translates in a 13% uncertainty on the measured thickness. In fact, the declared uncertainty for the instrument is 1 ÷ 5% for thicknesses larger than 0.5 μm. This uncertainty must be increased because of errors connected to the difficult determination of craters and their measurement at the optical microscope, and this gives indication on the confidence level to attribute to the most critical measurements (i.e. for the smallest thicknesses). As a comment to Table 1, we should notice that, for front and back faces of sample 62 a difference in thickness can be appreciated. However this difference can be considered as an effect of a wrong positioning of the sample within the bath, i.e. with the electrode closer to the front face, as the mean value of thickness fairly agrees with other samples.

3.2. Surface characterization

The surface roughness has been investigated and the results are summarized in Table 2. We can see that the roughness *Rz* generally decreases as the Cu thickness increases.

The evidenced roughness decrease can also be qualitatively evaluated from SEM images shown in Figs. 4–6. All images have been taken with 15.0 kV accelerating voltage and 10000× magnification. Cu crystals can be easily recognized on the surfaces.

To analyze the effect of the current density on the sample morphology, we consider samples with comparable thicknesses produced by different current densities. An example is the couple 58b (Fig. 4) - 74f (Fig. 5, sample obtained with a lower current density). We can see that at lower current densities (i.e. at longer deposition times) crystals with larger average dimensions and with a better uniformity of dimensions and positions can be obtained, thus producing an overall lower surface roughness. On the other hand, if we consider, at fixed current density the effect of deposition time, we can see that *Rz*

Table 2
Surface roughness of significant samples. *Rz* labels the average value of 5 maximum height differences measured on 5 portions next to the measured profile. Last two lines list the data for samples obtained with J = 0.51 A dm^{-2}.

Sample	Thickness Ni μm	Rz μm
AISI 304	0	2.2
70f	0.37	1.6
58b	0.47	1.8
438b	0.84	1.2
63f	1.36	1.2
442f	1.49	0.6
446f	1.69	0.6
450f	4.14	0.6
454b	7.38	0.8
74f	0.52	1.7
460f	1.47	0.6

initially decreases with increasing time, reaching a minimum value of 0.5 at 1.7 μm thickness. Then, its value remains nearly constant up to 4 μm thickness. Any further thickness increase above this value produces also an increasing of *Rz*. Fig. 6, showing the SEM image of sample 454b can explain this behavior: if the deposition time increases, the dimensions of Cu crystals considerably increase, but their dimensions tend to become less uniform. In fact in Fig. 6 we can appreciate even 1–2 μm crystals, value that can explain the increase of *Rz*.

3.3. Optical characterization

Fig. 7 shows the hemispherical reflectance spectra in the range 0.25–16 μm for the most significant samples. By comparing the spectra of different samples, the most significant parameter affecting optical properties seems to be the surface roughness, while the effect of the coating thickness appears of lower importance. In fact, samples with the same or similar roughness (438b - 63f, roughness 1.2 μm and 442f - 446f - 450f - 454f roughness 0.6–0.8 μm) show very similar spectra, even if the thickness of the coating is different or very different (0.8–1.4 μm and 1.5–7.4 μm respectively within the two groups). The anomalous reflectance decrease for 438b sample for wavelengths longer than about 2 μm needs additional investigations and could be likely ascribed to surface degradation. As for surface oxidation, it should be noticed that in the finished solar absorber the Cu layer is covered by the sunlight absorbing black layer. This protects copper from the contact with oxygen and thus from oxidation. For this reason, oxidation issues have been not taken into account in the present work.

Fig. 8 compares the reflectance spectra of samples coated at different current densities and similar thicknesses (samples 58b vs. 74f, thickness ≃ 0.5 μm and 446f vs. 460f, thickness ≃ 1.6 μm). Moreover, it should be noticed that within each couple, also the roughness is similar (2.0–1.8 μm for 58b - 74f and 0.5–0.7 μm for 446f - 460f). Samples 58b e 446f have been obtained with J = 3.45 A dm^{-2}, while samples 74f e 460f with J = 0.51 A dm^{-2}. Sample 74f shows an absorption peak around 15 μm likely due to oxides on the surface. We can appreciate that, despite the different thickness, samples 74f and 460f, obtained with the same, lower, current density, show very similar spectra, except for the already described absorption peak at 15 μm. As for the comparison between samples with similar thickness, the largest spectral differences are referred to the visible-near infrared wavelength range (i.e. for wavelength shorter than 1 μm), while at longer wavelengths the spectra are nearly superimposed. The largest spectral differences within each couple are evidenced for samples 446f and 460f and are mainly concentrated in the 0.5–0.8 μm wavelength region (the smoother 446f sample also has the highest reflectance in this region). It should be noticed that the roughness values of these samples are 0.5 and 0.7 μm, respectively. Thus we can infer that major effects of roughness on the spectra can be expected in spectral regions where the roughness value is comparable to light wavelength. When roughness value becomes lower than light wavelength, almost all samples are seen as equally smooth by the incoming light and the spectra become practically superimposed, as it happens for wavelengths above 2 μm. The same qualitative behavior is confirmed by the spectra shown in Fig. 7.

To correlate (if possible) the Cu thickness to optical properties for solar applications, we calculated the sample thermal emittance at T = 300 °C using Eq. (1)

$$\varepsilon = \frac{\int_{\lambda_1}^{\lambda_2} (1 - R_\lambda) B_{\lambda,T} \mathrm{d}\lambda}{\int_{\lambda_1}^{\lambda_2} B_{\lambda,T} \mathrm{d}\lambda} \tag{1}$$

with integration bounds $\lambda_1 = 0.25$ μm and $\lambda_2 = 16$ μm. The calculated emittance for each sample is shown in Fig. 9.

From Fig. 9 we cannot correlate ε_T and thickness, as ε_T values are extremely spread for all the considered thicknesses. Moreover, we can observe that the average emittance is around 0.06, a value which is comparable with that obtained for

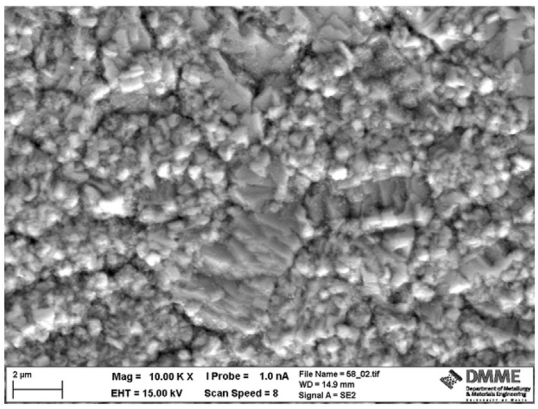

Fig. 4. Surface of sample 58b.

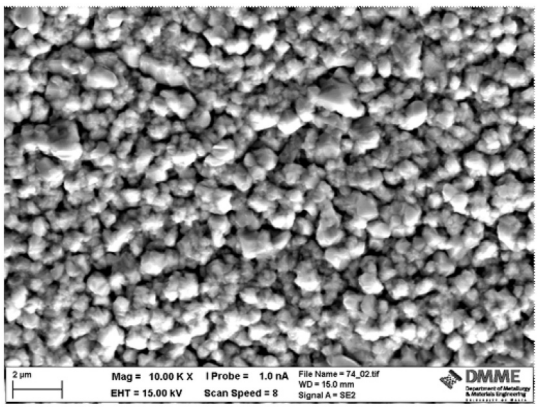

Fig. 5. Surface of sample 74f.

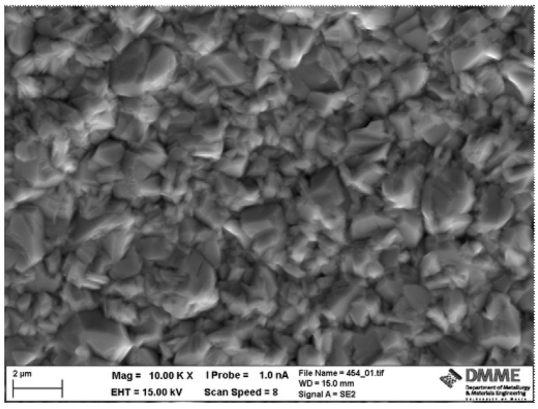

Fig. 6. Surface of sample 454b.

Wood nickel coating [21] (that, however, has the advantage to be much more reproducible). On the other hand, Cu coatings have the advantage over Ni of allowing a much easier black chrome deposition, with a more homogeneous Cr layer on the final product. The dispersion of ε_T values for Cu coatings can be likely due to the intrinsic quick oxidation of copper. In fact, even during the small time gone between sample production and optical measurement (few days) some oxidation could be observed. However this problem can be easily avoided for an hypothetical industrial production line of a Cu-based substrate

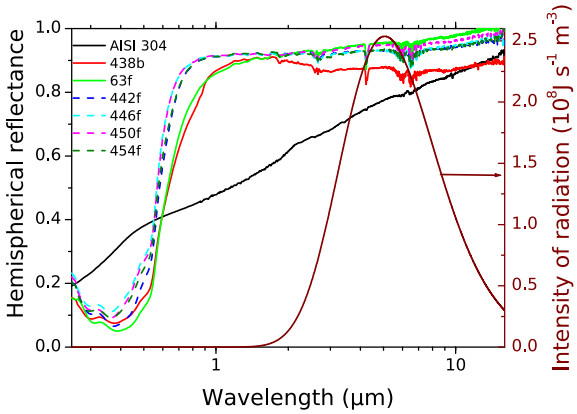

Fig. 7. Comparison of reflectance spectra of several Cu-coated samples and of the bare AISI 304 substrate. Legend lists the sample labels, sorted as a function of increasing deposition time (and thus increasing thickness). The blackbody emission at 300 °C is also shown for reference.

for black chrome, as the sunlight absorbing coating would be deposed, in that case, immediately after the Cu deposition, thus efficiently protecting it from oxidation.

3.4. Optical characterization in far IR

For sake of completeness, we acquired also mid- and far-infrared specular reflectance spectra from 16 to 40 μm wavelength for some representative samples, to assess optical properties at longer wavelengths and check the sample purity. The specular reflectance in the range 0.25–40 μm is shown in Fig. 10. As expected, specular reflectance values are lower than the hemispherical ones, with decreasing differences as the sample roughness decreases. The spectra appear smooth, with reflectance values growing towards the infrared and generally characterized by a high-reflectance plateau around 90% appearing in the majority of the investigated spectral range. It seems reasonable to expect a similar trend also for hemispherical reflectance, i.e. spectra asymptotically tending to 100% reflectance within the experimentally available spectral range. Thus, due to the spectral distribution of the blackbody emission, which is near to zero at 40 μm wavelength, we can expect a substantial confirmation of the emittance results discussed in the previous section. In fact, the unknown region could reasonably produce only a constant offset in the calculation of Eq. (1) for all samples. As for far-infrared characteristics of the spectra, similarly to what already observed for Fig. 7, also the curves shown in Fig. 10 are affected by surface roughness effects. In fact, samples with the same or similar roughness (70f - 58b - 74f, roughness 1.6 ÷ 1.8 μm and 442f - 450f roughness 0.6 μm) show similar spectra, and the group with lower roughness is characterized by a higher reflectance. The sample 70f shows some deviations from the almost perfectly straight plateau at long wavelengths. This behavior needs additional investigations and could be ascribed to oxidation or sample contamination.

4. Conclusions

In this work we report on the production, structural and optical characterization of copper coatings deposed on Ni-coated stainless steel substrates. The investigated samples are intended as substrate for a further black chrome deposition, in the perspective to produce optimized solar absorbers for parabolic trough collectors (PTCs). Good repeatability of the electrodeposition bath has been found, with a linear dependence of the coating thickness on both deposition time and current density. The hemispherical reflectance spectrum, measured from 0.25 to 16 μm wavelength region, has been found to be mainly dependent on the sample roughness. As for the effect of deposition parameters, lower current densities and longer deposition times generally arise in more homogeneous surfaces, with lower roughness and thus higher reflectance. As for optical properties, a low thermal emittance is the most significant characteristics required to substrates for black chrome, so that the final device will merge optimal sunlight absorption properties supplied by the exterior black layer to minimal thermal losses assured by the inner coating. Thus we calculated the thermal emittance at 300 °C temperature from experimental spectra. In spite of dispersed values likely due to the intrinsic quick oxidation of copper, which, however, can be easily avoided in hypothetical future industrial production lines, an emittance value of about 0.06 could be inferred. This value is similar to that obtained from previous studies on Wood nickel coating. Despite this disadvantage, the copper layer is interesting because it is easy to deposit and the process is more efficient than the Wood process. Another parameter to take into account is the working temperature in order to prevent interdiffusion in other metal layers [24,17]. However this is not a problem in the operating range of mid-temperatures PTC (200 ÷ 300 °C).

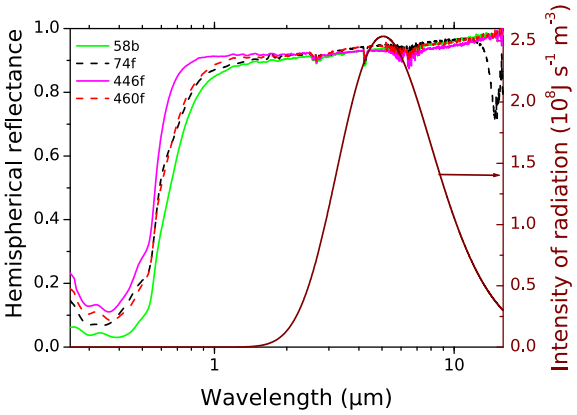

Fig. 8. Comparison of reflectance spectra of samples coated at different current densities and with comparable coating thicknesses. The blackbody emission at 300 °C is also shown for reference.

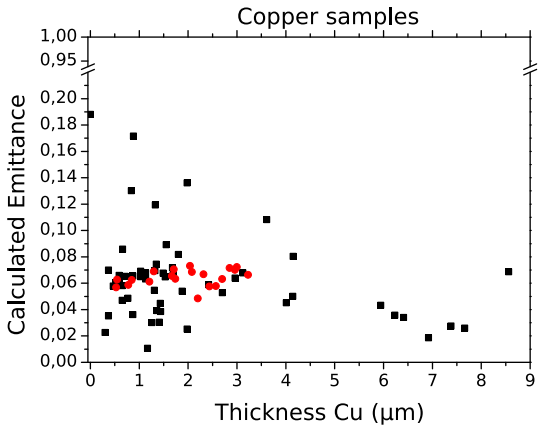

Fig. 9. Emittance of Copper samples as a function of thickness (black squares). The emittance of AISI 304, taken as reference, is shown at 0 μm thickness. For comparison, red dots show the data of Wood-type Nickel coatings [21]. (For interpretation of the references to colour in this figure legend, the reader is referred to the web version of this article.)

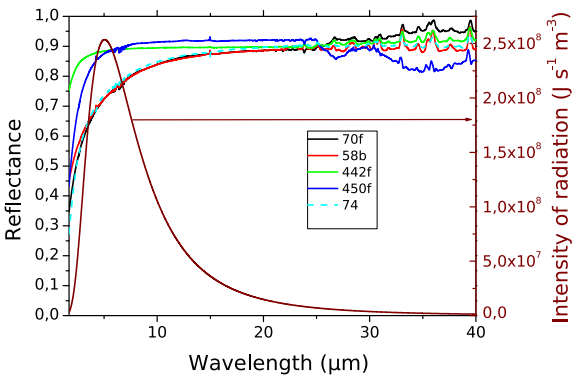

Fig. 10. Comparison of specular reflectance spectra of several Cu-coated samples. Legend lists the sample labels, sorted as a function of increasing deposition time (and thus increasing thickness). It is also sown sample 74f obtained at lower current density. Picture also shows in wine colour the blackbody spectrum at 300 °C.

Acknowledgments

E.S. gratefully acknowledges the Italian bank foundation “Fondazione Ente Cassa di Risparmio di Firenze” for providing the grant for M.M. within the framework of the “SOLE” and “SOLE-2” projects (pratiche n. 2013.0726 and 2014.0711). Authors thank Dr. Stefano Caporali for help for the thickness measurements, Dr. James Camilleri and Prof. Jonathan Betts for the SEM images.

References

[1] Soteris A. Kalogirou, Solar thermal collectors and applications, Prog. Energy Combust. Sci. 30 (3) (2004) 231–295.
[2] C.E. Kennedy, Review of Mid-to-high Temperature Solar Selective Absorber Materials, National Renewable Energy Laboratory, 2002.
[3] H. Yüncü, E. Paykoc, Y. Yener (Eds.), Solar Energy Utilization: Fundamentals and Applications, vol. 129, Springer Science & Business Media, 2012.
[4] Wenhua Yu, David M. France, Jules L. Routbort, Stephen US. Choi, Review and comparison of nanofluid thermal conductivity and heat transfer enhancements, Heat. Transf. Eng. 29 (5) (2008) 432–460.
[5] E. Sani, S. Barison, C. Pagura, L. Mercatelli, P. Sansoni, D. Fontani, D. Jafrancesco, F. Francini, Carbon nanohorns-based nanofluids as direct sunlight absorbers, Opt. Express 18 (5) (Mar 2010) 5179–5187.
[6] E. Sani, L. Mercatelli, S. Barison, C. Pagura, F. Agresti, L. Colla, P. Sansoni, Potential of carbon nanohorn-based suspensions for solar thermal collectors, Sol. Energy Mater. Sol. Cells 95 (2011) 2994–3000, http://dx.doi.org/10.1016/j.solmat.2011.06.011.
[7] A. Moradi, E. Sani, M. Simonetti, F. Francini, E. Chiavazzo, P. Asinari, Carbon-nanohorn based nanofluids for a direct absorption solar collector for civil application, J. Nanosci. Nanotechnol. 15 (2015) 3488–3495, http://dx.doi.org/10.1166/jnn.2015.9837.
[8] E. Sani, P. Di Ninni, L. Colla, S. Barison, F. Agresti, Optical properties of mixed nanofluids containing carbon nanohorns and silver nanoparticles for solar energy applications, J. Nanosci. Nanotechnol. 15 (2015) 3568–3573, http://dx.doi.org/10.1166/jnn.2015.9838.
[9] R. Mondragon, R.O. Torres-Mendieta, M. Meucci, G. Mínguez-Vega, J.E. Juliá, E. Sani, Synthesis and characterization of gold/water nanofluids suitable for thermal applications produced by femtosecond laser radiation, J. Photonics Energy 6 (3) (July 19, 2016), http://dx.doi.org/10.1117/1.JPE.6.034001, 034001.
[10] G. Gukhman, M. Koltun, A. Gavrilina, Stable selective coating black nickel for solar collector surfaces, Sol. Energy Mater. Sol. Cells 33 (1) (1994) 41–44.
[11] Ewa Wäckelgård, Characterization of black nickel solar absorber coatings electroplated, Sol. Energy Mater. Sol. Cells 56 (1) (1998) 35–44.
[12] S.N. Patel, O.T. Inal, A.J. Singh, A. Scherer, Optimization and thermal degradation study of black nickel solar collector coatings, Sol. Energy Mater. 11 (1985) 381–399.
[13] M.R. Bayati, M.H. Shariat, K. Janghorban, Design of chemical composition and optimum working conditions for trivalent black chromium electroplating bath used for solar thermal collectors, Renew. Energy 30 (14) (2005) 2163–2178.
[14] Glen E. McDonald, Spectral reflectance properties of black chrome for use as a solar selective coating, Sol. Energy 17 (2) (1975) 119–122.
[15] P.M. Driver, An electrochemical approach to the characterisation of black chrome selective surfaces, Sol. Energy Mater. 4 (2) (1981) 179–202.
[16] A. Muehlratzer, G.P. Goerler, E. Erben, H. Zeilinger, Selection of a black chrome bath for continuous tube-plating and the properties of the coatings deposited from it, Sol. Energy 27 (2) (1981) 115–120.
[17] Kil Dong Lee, Won Chae Jung, Jong Heon Kim, Thermal degradation of black chrome coatings, Sol. Energy Mater. Sol. Cells 63 (2) (2000) 125–137.
[18] R.B. Pettit, R.R. Sowell, I.J. Hall, Black chrome solar selective coatings optimized for high temperature applications, Sol. Energy Mater. 7 (2) (1982) 153–170.
[19] Nenad V. Mandich, Donald L. Snyder, Electrodeposition of Chromium, John Wiley & Sons, Inc, 2010, pp. 205–248.
[20] Walter F. Bogaerts, Carl M. Lampert, Materials for photothermal solar energy conversion, J. Mater. Sci. 18 (1983) 2847–2875, http://dx.doi.org/10.1007/BF00700767.
[21] S. Pratesi, E. Sani, M. De Lucia, Optical and structural characterization of nickel coatings for solar collector receivers, Int. J. Photoenergy (2014) 7, http://dx.doi.org/10.1155/2014/834128. Article ID 834128.
[22] R. Cloots, V. Moise, A. Rulmont, Study of the electrochemical synthesis of selective black coatings absorbing solar energy, Int. J. Inorg. Mater. 3 (8) (2001) 1323–1329.
[23] J.M. Behaghel, J. Lafait, S. Berthier, Le chrome noir et la sélectivité aux moyennes températures (100-250 °C), Rev. Phys. Appl. (Paris) 15 (1980) 403–409, http://dx.doi.org/10.1051/rphysap:01980001503040300.
[24] Carl M. Lampert, Jack Washburn, Microstructure of a black chrome solar selective absorber, Sol. Energy Mater. 1 (12) (1979) 81–92.
[25] David Hopwood, 81st Metal Finishing Guidebook, vol. 844, 2013.
[26] J.R. Davis, A.S.M.I.H. Committee, Copper and Copper Alloys, in: ASM Specialty Handbook, ASM International, 2001.
[27] E. Bertorelle, Trattato di galvanotecnica, 1977.